

Chemical compositions of semi-regular variable red giants

Ramyapoath* and David L. Lambert†

The W.J. McDonald Observatory & The Department of Astronomy, The University of Texas at Austin, Austin, TX 78712, USA

Accepted XXX. Received YYY; in original form ZZZ

ABSTRACT

A sample of warm low level semi-regular variables chosen from the *General Catalogue of Variable Stars* is studied for their chemical compositions by analysing high resolution optical spectra. The abundance ratios from Na/Fe to Eu/Fe displayed by these and previously analysed semi-regular variables are quite similar to ratios displayed by normal red giants across the Galactic thin and thick disks and halo populations in the solar neighbourhood suggesting from this perspective that the variables may be among the more photometrically active red giants.

Key words: stars: abundances — stars: variables — stars: fundamental parameters — stars: late-type

1 INTRODUCTION

The *General Catalogue of Variable Stars* defines the SRd class to be composed of ‘Semiregular variable giants and supergiants of F, G or K spectral types, sometimes with emission lines in their spectra. Amplitudes of light variations are in the range from 0.1 to 0.4 mag and the range of periods is from 50 to 1100 days’ (Samus’ et al. 2017). Our present selection of SRd and SRd: variables observed for spectroscopic analysis and discussion is drawn from the 2022 June version of the *GCVS*.¹ Assignment to the SRd: class exploits the traditional astronomical use of a colon to indicate a variable very likely similar to a SRd variable but presumably of less certain photometric variability with respect to amplitude and/or period. The *GCVS* catalogue consulted by us lists 177 SRd and 100 SRd: variables. Among the listed variables from the *GCVS* are supergiants – evolved massive stars – such as R Pup and ρ Cas. Another subsample are post-AGB low mass stars such as 89 Her and UU Her with their fascinating spectroscopic signatures. But the majority of SRd and SRd: variables appear to be lower-mass giants associated with the Red Giant Branch (RGB) including cooler and more luminous giants extending into the M spectral types and thus populating the upper reaches of the RGB to its tip where He is ignited in the star’s interior and the star quickly assumes the identity of a red clump (RC) giant before evolving to the AGB. Giants on the RC and the AGB also fall within the SRd and SRd: domain. Our

emphasis here is on RGB, RC and early-AGB giants, more specifically excluding stars with spectra in which TiO bands are prominent, i.e., our sample excludes M-type giants.

Identification of a red giant as a variable is dependent on its photometric variability and, of course, also on a capability to detect this variability. Early additions to the SRd and SRd: lists of red giants often exhibited a visual magnitude amplitude of 1 magnitude or more and a spectral type variation, say typically G2 to K2 with excursion into the M giants. Variability linked to radial pulsations fed by asteroseismology is of low amplitude in K giants but increases in M giants. Other and speculative triggers for variability may exist such as a close stellar companion or near-merging planet, a magnetic field and the stimulus resulting from He-core ignition at the RGB tip which may persist for a time in an AGB giant.

In this paper, we explore the similarity between a collection of SRd (SRd:) variables and non-variable red giants with respect to chemical composition as anticipated from their stage of evolution and Galactic kinematics. Our variable giants include stars of differing metallicities. The Galactic characteristics of the variable and non-variable giants range from thin disk to thick disk to halo. Our high-resolution optical spectra were collected over the years as gaps arose in our other observing programmes undertaken at the W.J. McDonald Observatory. The principal goal was to search for anomalies – chemical or kinematical – relative to red giants not (yet?) labelled as variable.

2 OUR SAMPLE OF SEMI-VARIABLE RED GIANTS

Our observed SRd and SRd: variables drawn from the *GCVS* electronic catalogue were sifted to reject the few stars that

* e-mail: ramyap09@gmail.com

† e-mail: dll@astro.as.utexas.edu

¹ Caution! The electronic *GCVS* does not recognize lower case letters and, for example, identifies a SRd as a SRD variable. We prefer the designation SRd but occasionally employ SRD believing the reader will appreciate their equivalence.

were not red giants and those variables with TiO bands in their spectrum. The analysed sample (Table 1) is dominated by K giants with typical line widths indicating a pairing of a low projected rotational velocity with typical turbulence (i.e., an Arcturus-looking optical spectrum). The Table 1 entries include the name and variable type from the *GCVS*, the HIP number (Perryman et al. 1997) or an alternative identifier, the range in brightness with the minimum and maximum magnitudes which includes *Hipparcos* magnitudes Hp or other entries such as the visual, photovisual or Johnson *V* magnitude range and the photographic magnitude *p*, taken from the *GCVS*. The Table’s final column provides either the period of the variability from the *Hipparcos* entry or that catalogue’s characterization of the variability: C = constant, M= possible microvariable with an amplitude of less than 0.03 mag. and U = unsolved (uncertain?) variable which does not fall in the other categories, which also includes irregular or semi-regular variables, and possibly variables with amplitude not exceeding 0.03 mag. In two cases, the period of variability is taken from the *GCVS*. Of the entries in Table 1, ten were listed as *GCVS* variables following *Hipparcos*.

Approximately half of the variable red giants observed at McDonald provided spectra with TiO bands present to differing degrees. In some cases, the TiO bands may range from absent to prominent as a star executes its variation – see, for example, the case of W LMi (Giridhar et al. (2000), Fig. 2). TiO bands are an additional challenge to the quantitative spectroscopist. Giridhar et al. (2000) analysed a spectrum of AG Aur in which TiO bands were ‘strong’ to find a near-normal mix of elements but some elements were inaccessible thanks to line blending and some were unusually uncertain, as judged by their [M/Fe] index. Here, we post-pone analysis of those variables exhibiting TiO bands.

Three additional variables observed at McDonald – V897 Her, V395 Cyg and OX Ser – are not listed in Table 1. Each is unusually broad-lined suggestive of a high projected rotational velocity. We have not proceeded with a detailed abundance analysis of the trio in light of the inevitably lower accuracy of [M/Fe] indices for these broad-lined stars.

In later interpretation of compositions of semi-regular red giants, we extend the sample to include variables previously reported in the literature as having spectroscopically-determined chemical compositions. The chosen analyses are considered to be generally similar in precision to ours. This selection extends the size of the analyzed sample of SRd and SRd: red giants.

3 THE ROBERT G. TULL SPECTRA

High-resolution optical spectra of semi-regular variables were observed with the Tull coude echelle spectrograph at the 2.7 meter Harlan J. Smith Telescope of the W.J. McDonald Observatory (Tull et al. 1995) in breaks in observing runs dedicated to other projects. Variables were selected from the *GCVS* lists of SRd and SRd: variables (Samus’ et al. 2017).²

Spectra covered the interval 3800 to 10000 Å with

Table 1. Our SRd/SRd: sample.

Name	Type	Identifier	MinMag-MaxMag (GCVS)	Period (days)
V354 And	SRd:	HIP 2651	8.78-8.65(Hp)	U
AC Aqr	SRd	TIC 248564916	10.50-10.00(V)	68.0 ^a
LS Aqr	SRd:	HIP 114426	8.61-8.33(V)	U
AY Ari	SRd:	HIP 12600	6.84-6.82(V)	C ^b
EU Dra	SRd:	HIP 74280	8.76-8.56(V)	U
VW Dra	SRd:	HIP 84496	7.00-6.00(V)	
HP Eri	SRd:	HIP 21648	8.53-8.44(Hp)	U
V894 Her	SRd	HIP 80302	8.32-8.17(Hp)	U
V991 Her	SRd:	HIP 90417	9.98-9.33(Hp)	40.48
BN Lyn	SRd:	HIP 41075	4.27-4.21(V)	M
CD Psc	SRd:	HIP 1938	9.99-9.81(Hp)	37.21
EZ UMa	SRd:	HIP 46247	6.28-6.23(V)	U
KR Vir	SRd:	HIP 61899	9.65-9.39(Hp)	U
RX Vir	SRd:	TIC 96199381	9.10-8.70(p)	200.0 ^a

a : The photometric period is from the *GCVS*.

b : Henry et al. (2000)’s photometry suggests a 120 day period and an amplitude of 0.02 mag.

echelle orders incompletely recorded on the TK3 CCD longward of about 5800 Å. Wavelength calibration was provided by an exposure of a Th-Ar hollow-cathode lamp. Exposures of a flat-field lamp provided sensitivity and pixel-to-pixel calibration. The two-dimensional CCD exposures were reduced to a one-dimensional relative flux versus wavelength spectrum using the *Image Reduction and Analysis Facility (IRAF)*.³ The resolving power was 60,000 and the S/N ratio at the centre of an order contributing stellar absorption lines was typically 100 or greater.

4 ABUNDANCE ANALYSIS OF THE VARIABLES

A LTE absorption line analysis was conducted employing model atmospheres and equivalent width analysis. All selected absorption lines were chosen from our ‘solar’ line list (Table 2 –see below). Atmospheric parameters – effective surface temperature (T_{eff}), surface gravity ($\log g$), microturbulent velocity (ξ_t) and metallicity ([M/H]) - were determined from a grid of model atmospheres. Kurucz model atmospheres with no convective overshoot were used. The code MOOG in its 2017 version was employed (Sneden 1973) in the procedure.

A selection of FeI and FeII lines were selected covering a range in excitation potential and equivalent widths (3mÅ– 175mÅ). The effective surface temperature T_{eff} was obtained by the method of excitation balance for FeI lines by zeroing the slope of the Fe abundance versus Lower Excitation Potential (LEP). The microturbulent velocity ξ_t was

³ *IRAF* is distributed by the National Optical Astronomy Observatory, which is operated by the Association of Universities for Research in Astronomy (AURA) under cooperative agreement with the National Science Foundation.

² *GCVS* database, Version 2022 June.

fixed by making the Fe I abundances independent of the line strength. Surface gravity $\log g$ was estimated demanding ionization balance, i.e., the Fe abundance from neutral and ionized Fe lines be the same. Finally, individual elemental abundances were estimated using the measured equivalent widths of the unblended spectral lines and the selected model atmosphere corresponding to the adopted stellar atmospheric parameters. For transitions with significant hyperfine splitting (Sc, V, Mn, Co, Ba and Eu), hyperfine corrections were applied using the *blends* driver in MOOG. The wavelengths and relative strengths of the hyperfine components were taken from Kurucz database except for Ba, for which they are taken from McWilliam (1998). The Sun provides a reference spectrum for our analysis. Also, we undertook an analysis of Arcturus, a red giant with atmospheric parameters similar to some of our variables. Our inferred composition of Arcturus is assessed relative to published analyses of the star.

4.1 The Sun and Arcturus

Our solar abundance analysis is based on the solar spectrum provided by Hinkle et al. (2000) and the Kurucz (1998) model solar atmosphere. Our line list in Table 2 was compiled from various sources, namely Bensby et al. (2003); Bubar & King (2010); Giridhar et al. (1994); Hekker & Meléndez (2007); Morel et al. (2014); Pompéia et al. (2011); Ramírez & Allende Prieto (2011); Ramya et al. (2019); Reddy et al. (2003), as well as the Kurucz database⁴. Hyperfine wavelength splittings were applied for Sc, V, Mn, Co, Ba and Eu. The Sun was considered using the 2017 version of the LTE spectral line analysis and spectrum synthesis code MOOG (Snedden 1973). Analysis of the line list gave the solar atmosphere parameters: temperature $T_{\text{eff}} = 5777$ K and surface gravity $\log g = 4.44$ cm s⁻² and microturbulent velocity $\xi_t = 1.14$ km s⁻¹.

Mean elemental abundances for each atom and ion with N , the number of contributing lines, are given in Table 3 which also gives Asplund et al. (2009) spectroscopic estimates for solar elemental abundances. The mean difference $|Current - Asplund|$ is a 0.03 ± 0.06 dex. Our iron abundance commonly adopted as ‘the solar metallicity’ is 7.44 ± 0.06 from the Fe I lines and 7.45 ± 0.06 from Fe II lines values slightly less than Asplund’s Fe abundance of 7.50 ± 0.04 . Our derived solar abundances are taken as the reference for the abundance analysis of the variable stars.

Since our investigation is directed at K giants, we sought to compare our results against those for the K giant Arcturus. In this study, we limit our study to elements above Na but anticipate studying lighter elements and their isotopes in a later exercise. For the Arcturus spectrum, we adopt that provided by Hinkle et al. (2000). Atmospheric parameters were derived from the atoms and ions well represented in our line list. These parameters given in Table 4 are the effective temperature (T_{eff}), the surface gravity (g , usually expressed as $\log g$), the microturbulence (ξ assumed to be isotropic and depth independent) and the composition ($[M/H]$ with relative elemental abundances taken to be solar). Our results and two reference results are given in Table 4. There may be some overlap in methods and stellar and

atomic data between the three analyses but, nonetheless, the close agreement between the analyses is pleasing.

Elemental abundances from our analysis are provided in Table 5 where we list $\log \epsilon(M)$ with its scatter σ and the number of measured lines N , the abundance ratio $[M/Fe]$ relative to the Sun. In the final columns, we give $[M/Fe]$ as determined by the reference studies in Table 4. Our abundances are consistent with previous studies: For example, the differences in $[M/Fe]$ between our analysis and that by Ramírez & Allende Prieto (2011) run from $+0.08$ to -0.12 for a mean of 0.00. A detailed comparison of the studies would be required to identify precise reasons for the small differences. All of the reported studies are based on an LTE analysis.

4.2 K giant semi-regular variables

Stars in Table 1 were observed and analysed. Atmospheric parameters for individual stars are given in Table 6. Elemental abundances as $[M/Fe]$ with their standard deviation and number of contributing lines are provided in Table 7. Iron abundances from Fe I and Fe II lines are both given relative to the solar Fe abundance. Also provided in the Tables is the assigned Galactic population – halo, thick or thin disk (see below). Uncertainties in the atmospheric parameters are estimated to be $\Delta T_{\text{eff}} = \pm 50$ K, $\Delta \log g = \pm 0.2$ dex, $\Delta \xi_t = \pm 0.2$ km s⁻¹, and $\Delta [M/H] = \pm 0.1$ dex (see Ramya et al. (2012) and Ramya et al. (2016)). The uncertainty in the abundances due to any parameter is estimated by measuring the amount by which the mean abundances vary responding to a change in the respective parameter by an amount equal to the uncertainty in the parameter, keeping the other parameters constant. Following the method, we estimated the resultant uncertainties in the abundances, $\sigma(T_{\text{eff}})$, $\sigma(\log g)$, $\sigma(\xi_t)$ and $\sigma([M/H])$ due to the uncertainties in the atmospheric parameters ΔT_{eff} , $\Delta \log g$, $\Delta \xi_t$ and $\Delta [M/H]$ respectively. The results obtained by applying this procedure to one of our sample stars AY Ari is given in Table 8. Assuming that the uncertainties in the parameters are unrelated and independent, the net uncertainty in the abundance ratio was calculated as a quadratic sum, which is given in the last column as $\sigma(\text{model})$. It is seen that the scatter for a given $[M/Fe]$ for AY Ari in Table 7 is similar to that from Table 8.

⁴ <https://lweb.cfa.harvard.edu/amp/ampdata/kurucz23/sekur.html>

Table 2: Our linelist

Ion	Wavelength (Å)	LEP (eV)	log gf	$W_{\lambda\odot}$ (mÅ)	log ε_{\odot} (dex)
Na I	6154.23	2.100	-1.550	36.6	6.26
	6160.75	2.100	-1.250	56.5	6.28
Mg I	5711.09	4.340	-1.730	104.1	7.56
	6318.72	5.110	-1.950	44.5	7.57
	6319.24	5.110	-2.320	27.4	7.63
	7657.61	5.110	-1.280	98.5	7.61
Al I	6696.02	3.140	-1.480	36.9	6.38
	6698.67	3.140	-1.780	20.8	6.33
	7835.31	4.020	-0.690	41.1	6.40
	7836.13	4.020	-0.450	55.0	6.36
Si I	5690.42	4.930	-1.770	48.1	7.45
	5701.10	4.930	-1.950	37.9	7.45
	5772.15	5.080	-1.650	52.3	7.54
	6142.49	5.620	-1.540	33.3	7.57
Ca I	6145.02	5.610	-1.479	37.6	7.58
	5260.39	2.520	-1.720	32.1	6.25
	5867.56	2.930	-1.570	22.6	6.25
	6166.44	2.520	-1.140	69.1	6.32
	6169.04	2.520	-0.800	90.3	6.34
	6169.56	2.530	-0.480	108.7	6.30
	6455.60	2.520	-1.340	55.9	6.27
	6471.66	2.530	-0.690	90.6	6.22
Sc II	6499.65	2.520	-0.820	84.7	6.25
	5357.20	1.510	-2.110	4.8	3.13
	5552.23	1.460	-2.280	4.6	3.22
	5684.21	1.510	-1.070	37.1	3.17
	6245.64	1.510	-1.040	35.2	3.08
	6300.75	1.510	-1.950	8.2	3.18
	6320.84	1.500	-1.920	8.9	3.18
	Ti I	5295.77	1.070	-1.580	13.2
5490.15		1.460	-0.880	22.0	4.84
5702.66		2.290	-0.590	7.3	4.78
5716.44		2.300	-0.720	5.9	4.82
6092.79		1.890	-1.320	4.1	4.84
6303.75		1.440	-1.510	8.8	4.93
6312.23		1.460	-1.500	8.1	4.90
6599.10		0.900	-2.030	9.3	4.92
Ti II	7357.73	1.440	-1.070	22.2	4.92
	4583.41	1.170	-2.870	33.0	5.02
	4708.66	1.240	-2.370	53.3	5.02
	5336.78	1.580	-1.630	71.7	4.96
V I	5418.77	1.580	-2.110	48.5	4.94
	6039.73	1.060	-0.650	12.3	3.87
	6081.44	1.050	-0.580	13.0	3.80
	6090.21	1.080	-0.060	32.3	3.83
	6119.53	1.060	-0.320	21.0	3.82
	6135.36	1.050	-0.750	10.2	3.85
Cr I	6274.65	0.270	-1.670	6.9	3.80
	5287.20	3.440	-0.890	11.3	5.61
	5300.74	0.980	-2.080	59.3	5.56
	5304.18	3.460	-0.680	16.0	5.59
	5628.62	3.420	-0.760	14.7	5.58
	5781.16	3.010	-1.000	16.7	5.49
Mn I	6882.48	3.440	-0.380	32.4	5.65
	6883.00	3.440	-0.420	30.5	5.64
	4671.69	2.890	-1.660	14.8	5.42
	4739.11	2.940	-0.600	60.7	5.36

	5004.89	2.920	-1.640	14.0	5.40
Fe I	5054.64	3.640	-2.140	39.1	7.55
	5088.16	4.150	-1.680	36.9	7.52
	5198.72	2.220	-2.140	94.9	7.36
	5253.02	2.280	-3.940	18.7	7.53
	5285.13	4.430	-1.640	27.9	7.54
	5294.55	3.640	-2.760	14.5	7.53
	5295.31	4.420	-1.590	28.5	7.49
	5322.00	2.280	-2.840	60.1	7.35
	5358.12	3.300	-3.162	9.50	7.39
	5379.57	3.690	-1.510	60.1	7.38
	5386.33	4.150	-1.670	31.4	7.38
	5441.34	4.310	-1.630	30.4	7.47
	5487.76	4.140	-0.710	86.8	7.49
	5543.94	4.220	-1.140	61.3	7.52
	5565.71	4.610	-0.230	84.4	7.35
	5569.63	3.420	-0.540	140.4	7.43
	5572.85	3.400	-0.310	172.0	7.45
	5576.10	3.430	-1.000	111.3	7.56
	5586.77	3.400	-0.210	194.9	7.51
	5522.45	4.209	-1.450	42.6	7.45
	5546.51	4.372	-1.210	50.5	7.51
	5560.21	4.430	-1.090	51.0	7.46
	5577.02	5.030	-1.550	11.5	7.50
	5661.35	4.280	-1.756	21.8	7.35
	5662.51	4.180	-0.570	89.9	7.43
	5638.26	4.220	-0.770	75.8	7.43
	5679.02	4.652	-0.750	58.2	7.45
	5618.63	4.209	-1.280	49.7	7.42
	5652.33	4.261	-1.850	26.1	7.54
	5701.55	2.560	-2.220	83.6	7.47
	5705.47	4.302	-1.500	37.7	7.48
	5731.76	4.260	-1.200	56.5	7.52
	5732.28	4.990	-1.560	14.1	7.58
	5753.13	4.260	-0.760	76.2	7.44
	5775.08	4.221	-1.141	58.4	7.46
	5778.45	2.588	-3.440	22.2	7.40
	5793.91	4.220	-1.619	33.2	7.42
	5849.69	3.695	-2.930	6.6	7.34
	5855.08	4.608	-1.478	21.0	7.35
	5856.10	4.294	-1.558	32.5	7.41
	5858.79	4.220	-2.180	12.5	7.40
	5859.60	4.550	-0.620	69.3	7.43
	5862.37	4.550	-0.420	82.4	7.46
	5902.47	4.593	-1.750	13.7	7.38
	5905.67	4.650	-0.690	56.8	7.36
	5916.25	2.453	-2.990	54.0	7.49
	5927.79	4.650	-0.990	41.5	7.36
	5929.68	4.550	-1.310	39.5	7.55
	5934.65	3.930	-1.170	73.2	7.50
	5984.83	4.710	-0.300	80.5	7.44
	6003.01	3.880	-1.060	81.7	7.49
	6008.54	3.870	-1.010	85.5	7.50
	6015.25	2.220	-4.680	5.10	7.52
	6024.07	4.530	-0.120	103.8	7.46
	6027.05	4.076	-1.300	63.2	7.56
	6056.00	4.730	-0.400	70.6	7.39
	6065.49	2.610	-1.530	114.4	7.34
	6078.49	4.796	-0.388	73.6	7.47
	6079.01	4.650	-1.020	44.9	7.46
	6093.64	4.607	-1.410	30.2	7.51
	6096.66	3.984	-1.810	36.9	7.46

6098.24	4.558	-1.800	15.8	7.46
6082.72	2.220	-3.570	34.0	7.43
6120.25	0.920	-5.950	5.2	7.49
6127.91	4.140	-1.400	47.6	7.41
6137.00	2.200	-2.950	65.2	7.42
6137.72	2.590	-1.400	123.0	7.31
6151.62	2.176	-3.300	48.7	7.40
6159.38	4.610	-1.830	12.6	7.42
6165.36	4.143	-1.460	43.9	7.40
6173.34	2.220	-2.880	67.0	7.40
6180.21	2.730	-2.650	53.3	7.40
6187.99	3.940	-1.620	46.1	7.40
6213.44	2.220	-2.480	81.7	7.31
6219.29	2.200	-2.430	87.9	7.36
6240.65	2.223	-3.287	47.8	7.41
6252.55	2.404	-1.891	118.3	7.55
6265.14	2.180	-2.550	85.2	7.40
6270.23	2.858	-2.540	51.6	7.37
6271.28	3.330	-2.703	23.8	7.41
6322.70	2.590	-2.430	74.5	7.47
6335.35	2.200	-2.350	96.0	7.42
6336.82	3.686	-0.856	100.9	7.42
6344.15	2.430	-2.920	61.4	7.52
6380.75	4.190	-1.380	50.5	7.49
6392.54	2.280	-4.030	17.8	7.53
6411.65	3.640	-0.720	120.6	7.52
6419.96	4.710	-0.240	81.3	7.38
6436.41	4.186	-2.360	10.0	7.42
6475.63	2.560	-2.940	54.4	7.52
6481.88	2.280	-2.980	63.0	7.46
6498.94	0.960	-4.690	45.4	7.47
6518.40	2.830	-2.460	56.2	7.35
6574.23	0.990	-5.000	27.7	7.45
6581.21	1.480	-4.680	20.8	7.45
6591.33	4.593	-1.950	10.5	7.42
6593.89	2.430	-2.420	83.8	7.46
6608.03	2.280	-4.030	17.2	7.50
6609.11	2.560	-2.690	64.0	7.46
6677.98	2.690	-1.470	121.0	7.39
6699.14	4.590	-2.100	7.9	7.42
6703.57	2.759	-3.023	36.1	7.42
6705.10	4.607	-0.980	45.4	7.37
6710.32	1.490	-4.870	15.1	7.47
6713.75	4.795	-1.400	20.8	7.42
6725.36	4.103	-2.167	17.0	7.41
6726.67	4.607	-1.030	46.0	7.43
6733.15	4.638	-1.400	25.9	7.40
6750.16	2.420	-2.620	72.7	7.41
6793.26	4.076	-2.326	12.4	7.37
6810.26	4.607	-0.986	48.6	7.43
6828.59	4.640	-0.820	54.6	7.41
6837.01	4.590	-1.687	17.6	7.41
6842.69	4.640	-1.220	39.1	7.51
6843.66	4.550	-0.830	59.5	7.43
6857.25	4.076	-2.038	22.3	7.40
6911.51	2.420	-4.040	13.3	7.50
6976.93	4.580	-1.850	16.5	7.53
6971.94	3.020	-3.340	12.6	7.36
6999.88	4.100	-1.460	53.8	7.51
7022.95	4.190	-1.150	63.6	7.48
7132.99	4.080	-1.650	42.1	7.45
7802.51	5.080	-1.310	15.4	7.39

	7807.92	4.990	-0.509	58.8	7.45
Fe II	4491.40	2.856	-2.700	77.5	7.51
	4508.29	2.856	-2.440	84.6	7.41
	4576.33	2.844	-2.950	63.4	7.39
	4620.52	2.830	-3.310	50.9	7.42
	4670.18	2.583	-4.090	30.8	7.48
	5197.57	3.230	-2.220	79.3	7.36
	5234.62	3.221	-2.180	83.3	7.39
	5256.92	2.890	-4.060	20.7	7.45
	5264.80	3.230	-3.130	47.9	7.53
	5325.60	3.220	-3.220	41.4	7.46
	5414.07	3.221	-3.580	27.5	7.47
	5425.26	3.200	-3.220	41.3	7.43
	5534.84	3.250	-2.750	58.0	7.40
	5991.38	3.150	-3.540	30.7	7.44
	6084.10	3.200	-3.780	20.6	7.45
	6113.32	3.220	-4.110	11.1	7.45
	6149.25	3.889	-2.630	35.7	7.36
	6247.54	3.890	-2.430	52.8	7.56
	6369.46	2.891	-4.110	19.4	7.45
	6416.93	3.890	-2.640	38.9	7.44
	6432.68	2.890	-3.690	40.7	7.57
	6456.39	3.903	-2.065	62.3	7.41
	6516.05	2.890	-3.310	52.3	7.45
	7515.83	3.900	-3.460	13.2	7.49
	7711.72	3.904	-2.555	46.1	7.49
Co I	5280.63	3.630	-0.030	20.3	4.82
	5352.04	3.580	0.060	25.1	4.79
	5647.23	2.280	-1.560	13.9	4.83
	6455.00	3.630	-0.250	14.8	4.82
Ni I	5088.96	3.678	-1.240	28.2	6.16
	5094.42	3.833	-1.074	30.4	6.19
	5115.40	3.834	-0.281	75.2	6.30
	6111.08	4.088	-0.808	33.6	6.20
	6130.14	4.266	-0.938	21.6	6.21
	6175.37	4.089	-0.550	47.7	6.23
	6176.80	4.090	-0.260	62.0	6.22
	6177.25	1.826	-3.508	14.1	6.17
	6772.32	3.658	-0.972	48.0	6.22
	7797.59	3.900	-0.348	75.3	6.29
	7826.77	3.700	-1.840	12.5	6.20
Zn I	4810.54	4.080	-0.170	71.6	4.48
	6362.35	5.790	0.140	21.2	4.52
Y II	5200.39	0.990	-0.570	36.3	2.10
	5289.82	1.030	-1.850	3.8	2.16
	5402.76	1.840	-0.620	11.6	2.24
	4883.67	1.080	0.070	56.5	2.07
	4982.11	1.030	-1.290	13.4	2.23
Zr I	4739.47	0.650	0.230	6.7	2.51
	6143.21	0.070	-1.100	2.3	2.68
Ba II	5853.68	0.604	-1.000	60.3	2.17
	6141.73	0.704	-0.032	109.1	2.31
La II	6390.48	0.320	-1.410	2.7	1.09
	4662.49	0.000	-1.240	7.0	1.14
	5303.54	0.320	-1.350	3.9	1.25
	6774.24	0.130	-1.820	2.6	1.27
Nd II	5319.81	0.550	-0.140	10.9	1.39
	5092.79	0.380	-0.610	5.5	1.37
	4989.92	0.630	-0.310	6.9	1.43
Eu II	6645.13	1.380	0.204	5.4	0.53

Table 3. The solar abundances.

Ion	N	Mean $\pm \sigma$ (dex)	Asp09 ^a (dex)	Mean-Asp09 (dex)
Na I	2	6.27 \pm 0.02	6.24 \pm 0.04	+0.03
Mg I	4	7.59 \pm 0.04	7.60 \pm 0.04	-0.01
Al I	4	6.37 \pm 0.03	6.45 \pm 0.03	-0.08
Si I	5	7.52 \pm 0.06	7.51 \pm 0.03	+0.01
Ca I	8	6.28 \pm 0.04	6.34 \pm 0.04	-0.06
Sc II	6	3.16 \pm 0.05	3.15 \pm 0.04	+0.01
Ti I	9	4.87 \pm 0.05	4.95 \pm 0.05	-0.08
Ti II	4	4.98 \pm 0.04		+0.03
V I	6	3.83 \pm 0.03	3.93 \pm 0.08	-0.10
Cr I	7	5.59 \pm 0.05	5.64 \pm 0.04	-0.05
Mn I	3	5.39 \pm 0.03	5.43 \pm 0.04	-0.04
Fe I	124	7.44 \pm 0.06	7.50 \pm 0.04	-0.06
Fe II	25	7.45 \pm 0.06		-0.05
Co I	4	4.81 \pm 0.02	4.99 \pm 0.07	-0.18
Ni I	11	6.22 \pm 0.05	6.22 \pm 0.04	0.00
Zn I	2	4.50 \pm 0.03	4.56 \pm 0.05	-0.06
Y II	5	2.16 \pm 0.07	2.21 \pm 0.05	-0.05
Zr I	2	2.59 \pm 0.12	2.58 \pm 0.04	+0.01
Ba II	2	2.24 \pm 0.10	2.18 \pm 0.09	+0.06
La II	4	1.19 \pm 0.09	1.10 \pm 0.04	+0.09
Nd II	3	1.40 \pm 0.03	1.42 \pm 0.04	-0.02
Eu II	1	0.53	0.52 \pm 0.04	+0.01

a : Asplund et al. (2009)

Table 4. Arcturus model stellar parameters

Parameter	Here	R&A11 ^a	Wo09 ^b
T _{eff} (K)	4285	4286	4300
log <i>g</i> (cm s ⁻²)	1.50	1.66	1.60
ξ_t (km s ⁻¹)	1.72	1.74	1.50
[M/H]	-0.59	-0.52	-0.60

a : Ramírez & Allende Prieto (2011)

b : Worley et al. (2009)

5 GALACTIC KINEMATICS OF THE VARIABLES

In broad terms, the stellar population in the solar neighbourhood is considered to arise from three components: the thin disk, the thick disk and the halo. These components are definable primarily by their Galactic velocity components U, V, W. In this section, we determine the components U, V, W for our variables and, also, for similar semi-variables stars with compositions reported previously in the literature. In a subsequent section, we assess whether our and comparable previously analysed variables have compositions expected of normal giants with the same Galactic kinematics.

Each population is represented by a three dimensional Gaussian distribution in the velocity space, with different dispersions along U, V and W. Adopting the kinematical

Table 5. Arcturus abundances.

Ion	log ϵ (M) and (N) Current study	[M/Fe]	[M/Fe] R&A11 ^a	[M/Fe] Wo09 ^b
Na I	5.81 \pm 0.01(2)	0.13	0.11 \pm 0.03	0.15 \pm 0.04
Mg I	7.41 \pm 0.02(4)	0.41	0.37 \pm 0.03	0.34 \pm 0.15
Al I	6.15 \pm 0.03(4)	0.37	0.34 \pm 0.03	0.25 \pm 0.07
Si I	7.24 \pm 0.08(5)	0.31	0.33 \pm 0.04	0.24 \pm 0.14
Ca I	5.84 \pm 0.03(8)	0.15	0.11 \pm 0.04	0.19 \pm 0.06
Sc II	2.66 \pm 0.04(6)	0.09	0.23 \pm 0.04	0.24 \pm 0.01
Ti I	4.51 \pm 0.07(9)	0.23	0.27 \pm 0.05	0.35 \pm 0.12
Ti II	4.54 \pm 0.04(4)	0.15	0.21 \pm 0.04	0.33 \pm 0.10
V I	3.32 \pm 0.03(6)	0.08	0.20 \pm 0.05	...
Cr I	5.00 \pm 0.09(7)	-0.01	-0.05 \pm 0.04	...
Mn I	4.63 \pm 0.01(3)	-0.18	-0.21 \pm 0.04	...
Fe I	6.85 \pm 0.08(122)	—	—	—
Fe II	6.87 \pm 0.07(25)	—	—	—
Co I	4.36 \pm 0.05(4)	0.14	0.09 \pm 0.04	...
Ni I	5.66 \pm 0.04(11)	0.03	0.06 \pm 0.03	...
Zn I	4.12 \pm 0.22(2)	0.21	0.22 \pm 0.06	-0.04 \pm 0.09
Y II	1.65 \pm 0.12(4)	0.08	...	0.12 \pm 0.11
Zr I	1.80 \pm 0.04(2)	-0.21	...	0.01 \pm 0.07
Zr II	1.97 \pm - (1)	-0.09	...	0.12 \pm 0.10
Ba II	1.51 \pm 0.19(2)	-0.15	...	-0.19 \pm 0.08
La II	0.47 \pm 0.09(4)	-0.14	...	0.04 \pm 0.08
Nd II	0.91 \pm 0.13(3)	0.10	...	0.10 \pm 0.07
Eu II	0.17 \pm - (1)	0.23	...	0.36 \pm 0.04

a : Ramírez & Allende Prieto (2011)

b : Worley et al. (2009)

properties for the thin disc, thick disk and halo distributions and the fraction of solar neighborhood stars belonging to each of these components from Table 1 of Reddy et al. (2006) (and references therein), we calculated the probability with which a star belongs to these three main components of the Galaxy. In a majority of cases, it was clear from the probabilities that the star's membership was assignable to one of the three Galactic population. Among our sample of variables, the majority belong to the thin disk but the thick and halo are represented.

Our calculations of U, V, W and the probabilities of membership are based on Gaia astrometric values (Gaia Collaboration et al. 2016, 2023; Babusiaux et al. 2023) but otherwise follow the recipe described by Reddy et al. (2006) which was based on *Hipparcos* not Gaia astrometric input. Gaia's DR3 values for the stellar parallax and proper motion but the radial velocity from our *Tull* spectrum were used in the computation of the U, V, W velocity components with respect to the Sun following the equations given in Johnson & Soderblom (1987). Population assignments would not be appreciably affected were the Gaia radial velocity preferred. Additionally, a variable surely has a somewhat variable radial velocity. A right-handed coordinate system is used where U is the radial component positive towards the Galactic center, V is the tangential component in the direction of Galactic rotation and W is the vertical component positive towards the North Galactic Pole. In general, disk kinematics imply large tangential or rotational velocities around the Galactic center (hence small with respect

Table 6. Derived atmospheric parameters for the sample stars grouped by Galactic population

Star	T_{eff} (K)	$\log g$ (cm s ⁻²)	ξ_t (km s ⁻¹)	[M/H] (dex)
Thin disk stars				
V354 And	4360	1.48	1.76	-0.27
AY Ari	4900	2.98	1.50	+0.31
EU Dra	4880	2.65	0.92	-0.35
VW Dra	4670	2.26	1.58	-0.05
V894 Her	4700	2.50	1.55	-0.12
V991 Her	4750	2.60	2.23	-0.15
BN Lyn	3910	0.98	1.54	+0.01
CD Psc	4930	2.52	1.81	-0.24
EZ UMa	4020	1.24	1.62	-0.16
RX Vir	5860	3.80	1.31	+0.13
Thick disk star				
AC Aqr	4220	0.07	2.13	-2.30
Halo stars				
LS Aqr	4030	0.10	2.13	-1.65
HP Eri	4310	0.52	2.16	-1.78
KR Vir	4060	0.05	2.36	-1.50

to Sun), while halo stars have the least rotational velocities around Galactic center and have highly eccentric orbits.

Table 9 provides the kinematical parameters for our warm variables. The sample is dominated by thin disk members (10 of 14) with the thick disk contributing just a single star and the halo three. Oddly, there is not a single entry with a mixed membership; presumably because our sample is too small. No attempt is made to search for kinematic structure within these Galactic populations. However, the thick disk’s representative AC Aqr seems unusually metal-poor at $[\text{Fe}/\text{H}] = -2.3$ for this population.

In considering variables drawn from the literature (see below), we use data from Gaia to compute velocities UVW and the above recipe to estimate probabilities of membership of Galactic halo, thick and thin disks.

6 PREVIOUSLY ANALYSED SRD VARIABLES

Our interest in previously analysed SRd-SRd: variables is (i) to compare results for stars in common with our sample in which previous authors adopted similar spectra and analytical techniques to us. Previous studies include those by Andrievsky et al. (1985, 2007), Giridhar et al. (1998, 1999, 2000), Britavskiy et al. (2010, 2012) and (ii) to extend the sample of variables with a known chemical composition. Several stars in previous studies – FT Cnc, XY Aqr, RX Cep and Z Aur – have now lost their SRd status in that they are not listed in the *GCVS* 2022 catalogue as SRd (or SRd:) variables. Such a revision of status is not surprising given the small amplitude of some photometric variations. In addition, ‘variable’ lacks a strict quantitative definition and, thus, is most difficult to apply to giant stars; all of which may be subject at a minimum to slight photometric varia-

tions of asteroseismic origin and, thus, are almost certainly variable when examined with precision.

Three of our variables were analysed previously from optical spectra: VW Dra (Britavskiy et al. 2012), V894 Her (Britavskiy et al. 2010) and RX Vir (Andrievsky et al. 2007). (RX Vir (see Table 6) is better linked to the main sequence than to the red giant branch but is a useful check on analytical procedures). The 2012 results and ours for VW Dra are in fine accord as to atmospheric parameters and to abundances [M/H]: the mean [M/H] difference between us and Britavskiy et al. (2012) is $\Delta = +0.01 \pm 0.14$ dex for 21 entries. Extremes contributing to this pleasingly small mean are -0.26 from Co I and $+0.37$ from Nd II. (For four light elements, Britavskiy et al. (2012) applied non-LTE corrections.) Similar remarks apply to the comparison between our results and Britavskiy et al. (2010): the mean $\Delta[\text{M}/\text{H}] = -0.09 \pm 0.21$ from 21 species with extremes -0.50 for Ti II and $+0.37$ for Nd II. With respect to [M/Fe], the mean difference would be increased to near zero by recognizing the overall difference in [Fe/H] between the analyses. Finally, the mean difference between our results and those of Andrievsky et al. (2007) for RX Vir is $\Delta[\text{M}/\text{H}] = +0.00 \pm 0.11$ dex for 18 entries.

It is of interest to examine recent large surveys of red giants, *LAMOST* and *APOGEE* (Majewski et al. 2017; Wilson et al. 2019; Gunn et al. 2006; Holtzman et al. 2010; Bowen & Vaughan 1973; Zasowski et al. 2017; Beaton, et al. 2021; Santana et al. 2021; Abdurro’uf et al. 2022) for additional SRd variables. Given the modest differences in [M/Fe] between disk and halo populations, we consider entries in the medium-resolution *LAMOST* catalogue but not the low-resolution *LAMOST* catalogues: then, the only SRds with reported *LAMOST* abundances are W LMi and HX Lyn. W LMi is the Li-rich variable on the AGB analysed previously by Giridhar et al. (2000). HX Lyn has not been previously analysed. For W LMi, the [Fe/H] and four [M/Fe] entries in common between the two studies are in satisfactory agreement. Our evaluation of the Galactic kinematics places HX Lyn with the thin disk and W LMi with the halo.

The most recent or DR17 *APOGEE* catalogue⁵ used here is based on the high-resolution H-band infrared spectra, the stellar parameters and chemical abundances derived using the Synspec (LTE) spectral synthesis code includes compositions of four SRd or SRd: variables among them AY Ari and RX Vir in Table 1. The mean [M/H] difference for AY Ari between us and *APOGEE* for [M/H] is $\Delta = -0.03 \pm 0.11$ dex for 13 entries. Similarly, the mean difference for RX Vir, the near-main sequence star, is $\Delta = -0.07 \pm 0.11$ dex for 11 entries. (An *APOGEE* catalogue is also provided with NLTE abundances for Na, Mg, K and Ca. NLTE corrections are estimated to be small.) These comparisons suggest that our abundance analysis and those provided by the *APOGEE* survey (García Pérez et al. 2016; Shetrone et al. 2015; Smith et al. 2021; Jönsson et al. 2020) are on the same scale. The *APOGEE* catalogue provides compositions for additional semi-regular variables with *GCVS* certification: QU Boo (thin disk) and V335 UMa (thin disk) with their Galactic population indicated.

⁵ https://data.sdss.org/sas/dr17/apogee/spectro/aspcap/dr17/synspec_lte/allStardr17synspec_lte.fits

Table 7. Derived abundances for the sample stars

	Thin disk stars						
	V354 And	AY Ari	EU Dra	VW Dra	V894 Her	V991 Her	BN Lyn
[Na I/Fe]	0.47 0.06 2	0.30 0.06 2	0.11 0.07 2	0.05 0.03 2	0.24 0.04 2	0.38 - 1	0.11 0.07 2
[Mg I/Fe]	0.03 0.06 2	-0.06 0.04 4	-0.08 0.16 2	0.12 0.07 4	0.08 0.06 3	0.28 0.12 2	0.03 0.04 4
[Al I/Fe]	0.31 0.09 4	0.07 0.05 4	0.20 0.06 4	0.15 0.03 4	0.23 0.03 4	0.36 0.09 3	0.11 0.06 4
[Si I/Fe]	0.02 0.10 4	0.06 0.09 5	0.02 0.09 5	0.11 0.07 5	0.05 0.05 5	0.38 0.08 2	0.22 0.12 5
[Ca I/Fe]	0.02 0.09 6	-0.05 0.07 8	0.01 0.09 8	0.02 0.04 8	0.13 0.06 8	0.34 0.06 5	-0.06 0.08 8
[Sc II/Fe]	-0.32 0.04 4	0.02 0.05 6	-0.31 0.04 2	-0.04 0.05 6	-0.08 0.06 6	0.06 0.04 2	-0.21 0.10 5
[Ti I/Fe]	-0.04 0.12 6	-0.05 0.07 7	0.03 0.1 5	0.01 0.07 7	0.05 0.08 6	0.36 0.12 5	-0.03 0.09 6
[Ti II/Fe]	-0.24 0.09 3	-0.17 0.1 4	-0.39 0.09 4	-0.08 0.06 4	-0.21 0.07 4	0.24 0.22 2	-0.27 0.07 4
[V I/Fe]	-0.04 0.07 5	-0.06 0.05 5	0.05 0.04 5	-0.02 0.04 5	0.04 0.06 5	0.33 0.11 5	0.14 0.08 5
[Cr I/Fe]	0.15 0.08 5	-0.01 0.06 6	0.12 0.12 7	0.01 0.08 6	0.14 0.06 6	0.08 0.12 4	-0.05 0.09 6
[Mn I/Fe]	-0.02 0.03 3	-0.07 0.05 3	-0.22 0.09 3	-0.08 0.1 3	-0.01 0.08 3	0.22 - 1	-0.34 0.04 3
[Fe I/H]	-0.27 0.11 84	0.30 0.08 112	-0.34 0.09 101	-0.03 0.08 103	-0.11 0.08 104	-0.13 0.13 63	-0.01 0.09 62
[Fe II/H]	-0.27 0.11 9	0.31 0.09 17	-0.33 0.06 8	-0.05 0.08 21	-0.12 0.09 23	-0.14 0.11 7	0.01 0.06 6
[Co I/Fe]	-0.10 0.07 4	-0.01 0.05 4	-0.16 0.08 4	0.00 0.05 4	-0.01 0.04 4	0.01 0.06 3	-0.12 0.07 4
[Ni I/Fe]	-0.03 0.08 10	0.06 0.07 11	-0.01 0.1 10	-0.01 0.06 11	-0.04 0.06 11	-0.04 0.07 8	-0.09 0.12 7
[Zn I/Fe]	0.14 0.05 2	0.07 0.1 2	0.06 0.04 2	0.10 0.08 2	0.06 0.11 2	-0.16 - 1	0.35 - 1
[Y II/Fe]	0.26 0.03 3	0.11 0.07 5	0.01 0.11 5	-0.07 0.06 5	0.27 0.14 5	0.17 0.14 2	0.90 0.06 2
[Zr I/Fe]	-0.19 0.11 2	-0.15 0.18 2	0.04 0.01 2	-0.24 0.09 2	-0.02 0.16 2	0.03 0.16 2	0.17 0.07 2
[Ba II/Fe]	0.26 0.18 2	0.07 0.16 2	0.37 0.08 2	0.11 0.18 2	0.28 0.23 2	-0.02 0.12 2	0.78 0.15 2
[La II/Fe]	-0.15 0.08 3	0.10 0.12 4	0.03 0.14 4	-0.04 0.09 4	-0.0 0.08 3	0.08 0.11 2	-0.15 0.10 3
[Nd II/Fe]	0.0 0.01 2	0.05 0.09 3	0.02 0.08 3	0.09 0.08 3	0.17 0.14 3	—	0.43 0.11 3
[Eu II/Fe]	—	0.10 - 1	—	0.17 - 1	0.04 - 1	—	0.09 - 1

	Thin disk stars			Thick disk star	Halo stars		
	CD Psc	EZ UMa	RX Vir	AC Aqr	LS Aqr	HP Eri	KR Vir
[Na I/Fe]	0.16 0.01 2	0.17 0.03 2	-0.10 0.05 2	—	0.04 0.02 2	—	-0.18 0.04 2
[Mg I/Fe]	0.13 0.06 2	0.08 0.07 4	-0.11 0.10 3	0.32 - 1	0.51 - 1	0.32 0.08 2	0.24 0.13 4
[Al I/Fe]	0.29 0.11 4	0.29 0.05 4	-0.09 0.02 4	0.80 0.09 2	0.32 0.07 3	—	0.04 - 1
[Si I/Fe]	0.10 0.08 4	0.17 0.05 5	-0.08 0.06 5	0.73 0.15 2	0.51 0.06 5	0.39 0.06 4	0.33 0.10 5
[Ca I/Fe]	0.11 0.08 7	0.02 0.07 8	0.01 0.07 7	0.32 0.09 6	0.28 0.04 8	0.27 0.01 6	0.18 0.06 7
[Sc II/Fe]	-0.14 - 1	-0.05 0.13 6	-0.13 0.07 5	-0.12 - 1	0.04 0.04 4	-0.13 0.04 4	-0.11 0.07 4
[Ti I/Fe]	0.15 0.09 2	0.00 0.08 6	-0.07 0.03 3	0.42 - 1	0.24 0.07 7	0.15 0.06 5	0.22 0.11 6
[Ti II/Fe]	0.10 0.11 2	-0.11 0.08 3	-0.06 0.05 4	0.44 0.09 4	0.33 0.10 4	0.32 0.08 4	0.30 0.10 4
[V I/Fe]	0.19 0.06 5	0.13 0.06 5	0.06 0.06 4	—	-0.08 0.07 6	-0.11 0.04 5	-0.06 0.07 5
[Cr I/Fe]	0.21 0.13 5	0.05 0.09 5	-0.02 0.07 5	-0.29 - 1	-0.18 0.10 3	-0.23 0.04 3	-0.36 0.11 2
[Mn I/Fe]	0.11 - 1	-0.38 0.07 3	-0.14 0.06 2	—	-0.30 - 1	—	-0.34 - 1
[Fe I/H]	-0.23 0.09 82	-0.16 0.11 88	0.14 0.08 111	-2.30 0.09 54	-1.66 0.09 90	-1.77 0.07 91	-1.50 0.09 81
[Fe II/H]	-0.24 0.09 9	-0.18 0.11 8	0.13 0.07 21	-2.29 0.04 9	-1.63 0.10 13	-1.77 0.08 13	-1.50 0.08 9
[Co I/Fe]	-0.06 0.11 3	-0.04 0.07 4	-0.01 0.08 4	—	0.06 0.09 3	0.03 0.02 2	-0.02 0.07 2
[Ni I/Fe]	-0.09 0.09 7	-0.04 0.10 9	-0.06 0.07 11	0.03 0.05 4	-0.11 0.04 9	-0.10 0.06 8	-0.19 0.08 8
[Zn I/Fe]	-0.15 - 1	0.50 - 1	-0.07 0.02 2	0.12 - 1	0.28 0.06 2	-0.01 - 1	0.00 - 1
[Y II/Fe]	0.29 0.12 3	0.49 0.08 2	0.10 0.07 5	-0.35 0.07 2	0.04 0.11 5	-0.10 0.10 4	0.11 0.06 3
[Zr I/Fe]	0.32 - 1	-0.16 0.16 2	—	—	0.02 0.07 2	0.18 0.09 2	0.01 0.01 2
[Ba II/Fe]	0.53 0.08 2	0.54 0.17 2	0.28 0.08 2	-0.29 0.12 2	-0.07 0.04 2	0.22 0.15 2	0.27 0.27 2
[La II/Fe]	0.27 0.06 2	-0.06 0.12 3	-0.01 0.12 3	-0.17 - 1	0.02 0.05 4	0.17 0.06 3	-0.05 0.07 4
[Nd II/Fe]	0.42 - 1	0.42 0.15 2	0.12 0.11 3	-0.15 0.10 3	0.12 0.09 3	0.27 0.08 3	0.13 0.08 3
[Eu II/Fe]	0.23 - 1	0.16 - 1	0.06 0.0 1	—	0.16 - 1	0.40 - 1	0.36 - 1

Thus, comparisons of abundance results for common stars suggest that our results from optical spectra and published results from *APOGEE* spectra are on very similar scales. This result encourages confidence that abundances for semi-regular variables – certainly, those derived from optical spectra free of TiO molecular lines – may be put up against trends for abundance trends within each of the Galactic kinematical populations to look for abnormali-

ties possibly related to the cause and execution of semi-regularity. Table 10 lists the previously observed and analysed variables chosen to enlarge the sample of semi-regular variables.

Table 8. Sensitivity of the abundances ($\Delta[M/Fe]$) to AY Ari’s atmospheric parameters.

Ion	$\sigma(T_{\text{eff}})$	$\sigma(\log g)$	$\sigma(\xi_t)$	$\sigma([M/H])$	$\sigma(\text{model})$
Na I	± 0.04	± 0.03	± 0.08	± 0.01	0.09
Mg I	± 0.02	± 0.01	± 0.05	± 0.01	0.06
Al I	± 0.03	± 0.02	± 0.05	± 0.01	0.06
Si I	± 0.03	± 0.02	± 0.04	± 0.02	0.06
Si II	± 0.11	± 0.04	± 0.04	0.0	0.12
Ca I	± 0.04	± 0.03	± 0.11	± 0.01	0.12
Sc II	± 0.01	± 0.08	± 0.03	± 0.04	0.09
Ti I	± 0.07	0.0	± 0.07	± 0.01	0.10
Ti II	± 0.01	± 0.06	± 0.11	± 0.03	0.13
V I	± 0.07	± 0.0	± 0.07	± 0.01	0.10
Cr I	± 0.04	± 0.01	± 0.09	± 0.01	0.10
Mn I	± 0.04	± 0.01	± 0.07	± 0.01	0.08
Fe I	± 0.02	± 0.01	± 0.10	± 0.01	0.10
Fe II	± 0.06	± 0.07	± 0.09	± 0.03	0.13
Co I	± 0.01	± 0.04	± 0.02	± 0.02	0.05
Ni I	0.0	± 0.02	± 0.10	± 0.02	0.10
Zn I	± 0.03	± 0.04	± 0.09	± 0.03	0.11
Y II	± 0.01	± 0.07	± 0.10	± 0.03	0.13
Zr I	± 0.08	± 0.0	± 0.05	± 0.01	0.09
Zr II	± 0.01	± 0.08	± 0.03	± 0.04	0.09
Ba II	± 0.01	± 0.06	± 0.25	± 0.03	0.26
La II	± 0.01	± 0.08	± 0.03	± 0.03	0.09
Nd II	± 0.01	± 0.08	± 0.06	± 0.04	0.11
Eu II	± 0.01	± 0.07	± 0.02	± 0.03	0.08

7 COMPOSITION OF GALACTIC HALO, THICK AND THIN DISK

The semi-regular variable red giants span a range in metallicity $[Fe/H]$ across the Galactic halo and the thin and thick disks with relative abundances $[M/Fe]$ differing in ways across the Galactic populations, as previously determined from abundance studies based on high-resolution optical spectroscopy of F and G dwarfs, for example, by Reddy et al. (2006) (and references therein) and of red giants, as, for example, collated by Nikos Prantzos and illustrated in the review by Arcones & Thielemann (2023). Our goal here is to test the idea that, warm semi-regular variable red giant stars may share the abundance pattern $[M/Fe]$ of normal red giant stars of the same Galactic population, i.e., the origin of the star’s semi-regularity appears not to have induced any anomalies in the abundances of observable elements Na and heavier. Our principal source of compositions for standard giant stars is the *APOGEE* catalogue which has been itself the source of investigations of the compositions of Galactic populations (for example, Imig et al. (2023); Weinberg et al. (2022)). The *APOGEE* catalogue is based on high-resolution H-band infrared spectra. Data from optical data might have served as a reference for the semi-variable stars. Collections of abundance data for giants and dwarfs in the solar neighbourhood drawn from optical spectra have been compared with abundance data from *APOGEE*. Jönsson et al. (2018) compare extensively several optical collections of abundance data with *APOGEE* data from data releases DR13 and DR14 and show that *APOGEE* - Optical abun-

dance systematics for our elements – Na, Mg, Al, Si, Ca, Cr, Mn and Ni – are less than 0.05 dex (median) and random differences are less than 0.15 dex (std. deviation).

The abundance pattern for giant stars drawn by us from *APOGEE* was based on a few selection rules: a high quality H-band spectrum selected making use of various flags – EXTRATARG flag, STARFLAG flag, SN_BAD bit and STAR_BAD bit of ASPCAP flag and also the bitmasks associated with the elemental abundances – provided in the catalogue, surface gravity $\log g \leq 3.0$, stars within 1 kpc of Sun with an error smaller than 10 % in their parallax. Galactic kinematics UVW were computed from Gaia DR3 entries and assignment to a particular Galactic population (halo, thick and thin disk) was assigned if the membership were calculated to be 90% or greater. This exercise resulted in a sample containing almost 4860 thin disk, just under 200 thick disk and almost two dozen halo giants. The entire sample (SRd variables and the *APOGEE* giants) spans the $[Fe/H]$ range from about +0.4 to almost -2.0 with the exception of the SRd AC Aqr at $[Fe/H] = -2.3$, which appears to be an odd thick disk representative.

Compositions for the different Galactic populations were examined in the $[M/Fe]$ vs $[Fe/H]$ plots. Our principal aim was to assess if the $[M/Fe]$ measures for the semi-regular variables follow the pattern of results for the *APOGEE* giants. *APOGEE* due to lack of absorption lines for heavy elements sampling *s*- and *r*-process elements is unavailable as an adequate reference for heavy elements. Hence, for heavy elements we drew on published abundances from optical spectra. Our intent here is *not* to interpret in the astrophysical sense the $[M/Fe]$ vs $[Fe/H]$ relations. Our primary aim is to address the question – do the variables in terms of their $[M/Fe]$ vs $[Fe/H]$ relations follow the relations exhibited by *APOGEE* giants spanning the same $[Fe/H]$ range?

Our selection of semi-regular variables does not extend to the extreme metal-poor halo giants. Yet, a potential indicator of an unusual nature for semi-regular variables would be a hint that slope of one or more of present trends of $[M/Fe]$ with $[Fe/H]$ suggest a $[M/Fe]$ mismatch with values obtained among extreme metal-poor halo giants. As representative of analyses of these halo giants, we consider Barklem et al. (2005)’s survey of abundance ratios for metal-poor halo stars which begins at about $[Fe/H] \simeq -1.5$ and extends down to -3.5 . For the many common elements between our two analyses, Barklem et al. (2005)’s $[M/Fe]$ at $[Fe/H] \simeq -2$ merge smoothly with the trends shown by semi-regular variable giants.

Although the sample Mg to Ni was examined individually, $[M/Fe]$ vs $[Fe/H]$ plots (Fig. 1 and Fig. 2) are shown only for M = Mg, Si, and Ca in Fig. 1 and M = Cr and Mn in Fig. 2. In these Figures, the thin disk giants selected from *APOGEE* DR17 (Synspec LTE) catalog are represented by yellow filled squares, the thick disk by yellow open diamonds and the halo by yellow filled triangles (A possibly common misapprehension is to identify the thin disk with the low $[Mg/H]$ vs $[Fe/H]$ strip and the high $[Mg/H]$ vs $[Fe/H]$ strip almost exclusively with the thick disk. But Fig. 1 following, for example, Imig et al. (2023) and Weinberg et al. (2022) shows the composition and kinematics of Galactic disk to be complex and, in particular, the composition of the thin disk appears to be binary in nature). Superimposed on each panel in these figures are results for the semi-regular vari-

Table 9. Kinematical parameters for the sample stars.

Star	v_{rad} (km/s) Gaia DR3	v_{rad} (km/s) (spec)	U (km/s)	V (km/s)	W (km/s)	P_{thin} (%)	P_{thick} (%)	P_{halo} (%)
Thin disk stars								
V354 And	-12.83±3.68	-7.6	-5.5 ± 0.5	-15.3 ± 0.8	-5.6 ± 0.4	99.2	0.8	0.0
AY Ari	22.01±0.13	21.5	-55.0 ± 0.8	-51.2 ± 0.5	-4.4 ± 0.4	96.5	3.4	0.1
EU Dra	-62.51±6.47 ^a	-57.2	28.1 ± 0.2	-49.0 ± 0.7	-28.4 ± 0.7	94.7	5.3	0.0
VW Dra	14.43±0.12	14.1	-11.2 ± 0.0	-2.7 ± 0.8	28.6 ± 0.6	95.6	4.4	0.0
V894 Her	-36.60±1.09	-40.3	-18.1 ± 0.6	-18.6 ± 0.5	-31.8 ± 0.7	98.0	2.0	0.0
V991 Her	-33.42±0.19	-33.1	10.6 ± 0.7	-64.5 ± 0.7	16.4 ± 0.2	88.8	11.1	0.1
BN Lyn	—	24.4	-32.0 ± 0.9	-50.8 ± 1.2	-0.4 ± 0.7	97.2	2.8	0.0
CD Psc	1.84±10.31	-5.1	-36.9 ± 0.6	-8.7 ± 0.5	9.8 ± 0.8	98.7	1.3	0.0
EZ UMa	16.38±1.18	9.8	-26.0 ± 0.7	-33.9 ± 0.6	8.5 ± 0.7	98.1	1.9	0.0
RX Vir	11.37±0.19	11.0	-30.6 ± 0.2	-16.3 ± 0.5	7.0 ± 0.8	98.8	1.2	0.0
Thick disk star								
AC Aqr	-5.37±0.77	-9.2	122.8 ± 10.7	-109.1 ± 8.6	9.0 ± 0.7	2.1	93.5	4.4
Halo stars								
LS Aqr	-311.56±0.67	-310.3	-22.1 ± 4.2	-255.0 ± 11.3	228.7 ± 4.1	0.0	0.0	100.0
HP Eri	19.89±0.25	18.4	168.2 ± 3.7	-137.7 ± 2.6	-145.5 ± 2.8	0.0	4.0	96.0
KR Vir	140.41±0.31	140.4	273.0 ± 10.8	-273.0 ± 9.6	-30.0 ± 6.9	0.0	0.0	100.0

a : Radial velocity of EU Dra is from Gaia DR2

Table 10. Previously analysed SRd stars.

Star	Type	[Fe/H]	Reference
Thin disk stars			
QU Boo	SRd	-0.33	APOGEE
V335 UMa	SRd:	-0.08	APOGEE
CW CVn	SRd	-0.14	Bri10 ^a
V463 Her	SRd	0.06	Bri10
MS Hya	SRd	-0.33	Bri10
MQ Hya	SRd	-0.12	Bri12 ^b
VV LMi	SRd	-0.14	Bri12
HX Lyn	SRd:	-0.483	LAMOST
Thick disk star			
WW Tau	SRd	-1.1	Gir00 ^c
Halo stars			
AB Leo	SRd	-1.96	And07 ^d
SV UMa	SRd	-1.87	And07
TY Vir	SRd	-1.71	And07
CK Vir	SRd	-1.88	And07
WY And	SRd	-1.0	Gir99 ^e
VW Eri	SRd	-1.8	Gir99
UW Lib	SRd	-1.3	Gir99
KK Aql	SRd	-1.2	Gir00
AG Aur	SRd	-1.7	Gir00
W LMi	SRd	-1.1	Gir00

a : (Britavskiy et al. 2010), b : (Britavskiy et al. 2012)

c : (Giridhar et al. 2000), d : (Andrievsky et al. 2007)

e : (Giridhar et al. 1999)

ables: blue and red symbols distinguish our variables from those previously analysed, as for the *APOGEE* giants, variables from the thin disk are represented by filled squares, thick disk members by open diamonds and halo representatives by filled triangles.

Fig. 1's value is that normal red giants as observed in *APOGEE* and earlier reported by many surveys show similar $[M/Fe]$ vs $[Fe/H]$ relations for $M = \text{Mg, Si and Ca}$ across the three Galactic populations with small scatter in the $[M/Fe]$ at a given $[Fe/H]$ in the halo. This common behaviour across the $[M/Fe]$ vs $[Fe/H]$ relations eases an identification of unusual results for the semi-variables. For $M = \text{Mg}$, semi-variables with the sole exception of the odd-appearing halo star AG Aur ($[Mg/Fe] = -0.4$ at $[Fe/H] = -1.8$ from Giridhar et al. (2000)) match satisfactorily the behaviour of the *APOGEE* halo giants. The optical spectrum of AG Aur was, as noted above, marred by TiO bands which may account for the low Mg abundance. The $[Si/Fe]$ panel shows a similarly tight distribution but for our thick disk giant AC Aqr with $[Si/Fe] = +0.73$ and three thin disk SRd variables (two from previous studies and our V991 Her) of above average $[Si/Fe]$. Ca shows a more severe introduction of unusually low $[Ca/Fe]$ for several $[Fe/H]$ -poor SRd variables including not only AG Aur. The other aberrant $[Ca/Fe]$ indices are from spectra with prominent TiO bands; presence of TiO bands in spectra of cooler semi-variables may result in additional unappreciated spectral complexity in optical spectra affecting line identification and measurement. Three thin disk variables exhibit $[Si/Fe]$ and $[Ca/Fe]$ of greater than normal indices but not apparently $[Mg/Fe]$: our V991 Her and the previously analysed MS Hya ((Britavskiy et al. 2010)) and VV LMi ((Britavskiy et al. 2012)).

Our second illustration involves Cr and Mn from the

iron group (Fig. 2). Both elements show a weak trend of $[M/Fe]$ with $[Fe/H]$. $[Cr/Fe]$ across the semi-regular variables which overlaps the weak tight trend displayed by the *APOGEE* giants. A few *APOGEE* giants have apparently unusually either high or low $[Cr/Fe]$. The sole previously observed SRd with even a mildly low $[Cr/Fe]$ is VV LMi at $[Fe/H] = -0.1$ with $[Cr/Fe] = -0.4$ with its Cr abundance based on 21 Cr I lines (Britavskiy et al. 2012)). Indeed, isolation of Cr in these plots is consistent with the assessment of the ‘reliability’ of *APOGEE* abundances⁶: Cr is identified as ‘less reliable’, Ca as ‘reliable’, and Mg, Si, Mn and Fe as ‘most reliable’.

Perhaps, the most puzzling example of an anomaly in the entire $[M/Fe]$ vs $[Fe/H]$ plane is provided by the four previously-observed halo variables at $[Fe/H] \sim -1.9$ with their remarkable $[Mn/Fe]$ about 0.7 dex less than the trend set by halo giants and halo variables at the same $[Fe/H]$. This quartet were provided by Andrievsky et al. (2007) who drew attention to them: “All [four] SRd program stars show uniform $[Mn/Fe]$ ratios that are typical for the stars with metallicity $[Fe/H] \simeq -3.5$. The reason for such a low Mn abundance in these stars is unknown.” For SV UMa, one of four variables, Giridhar et al. (1998) had reported a ‘near-normal’ $[Mn/Fe] = -0.2$ at $[Fe/H] = -1.4$ in disagreement with Andrievsky et al. as to Mn and Fe abundance. This Mn puzzle remains and warrants further spectroscopic examination. Barklem et al. (2005), as Andrievsky et al. (2007) noted, provide a map of $[Mn/Fe]$ in red giants to the Fe limit of the halo ($[Fe/H] \simeq -3.5$) which merges smoothly with the data in Fig. 2 less the troublesome quartet. The high $[Mn/Fe] = -0.2$ for the halo semi-variable KK Aql (Giridhar et al. 2000) also warrants additional investigation.

Agreement between compositions of semi-variable giants and regular giants (and dwarfs) extends to elements beyond the Fe-group. *APOGEE*’s selection of heavy elements is restricted to Ce so our comparisons are based on optical spectra. For thin disk semi-variable giants, our sample of seven provide a mean $[Eu/Fe] = 0.12 \pm 0.06$ in satisfactory agreement with the result from previously analysed variables giving $[Eu/Fe] = -0.08 \pm 0.12$ and in fine agreement with normal giants and F-G dwarfs (e.g., Reddy et al. (2006)) over the range $[Fe/H] \geq -0.5$. (CW CVn with $[Eu/Fe] = 0.64$ (Britavskiy et al. 2010) appears to be an anomaly). This agreement over $[Eu/Fe]$ estimates extends down close to $[Fe/H] \sim -1.0$ with the possible exception of W LMi at $[Fe/H] = -1.1$ where $[Eu/Fe] = +0.9$ (Giridhar et al. 2000) for this super Li-rich early-AGB variable. Eu is the classical indicator of an r -process contribution: thus, the r -process contribution at a given $[Fe/H]$ to normal dwarfs, giants and the semi-variable giants appears similar for the halo and the disks. For the measured heavy elements with an anticipated major origin from the s -process – Y, Zr, Ba and La with about 75% and Nd with 50% s -process to their solar abundance – the $[M/Fe]$ across the semi-variables and regular dwarfs and red giants is approximately flat but rising slightly at the lowest $[Fe/H]$ as the expected r -process contribution increases – say, from Y and Zr to Nd and Eu. Again, similar $[M/Fe]$ for semi-regular variables and ‘normal’ giants appears likely.

Inspection of Fig. 1 and Fig. 2 suggests that the compositions of semi-regular variables – analysed here and previously reported – closely resembles those of red giants as reported by *APOGEE*; both groups of giants share a common origin. Exceptions found among individual $[M/Fe]$ vs $[Fe/H]$ trends from both optically analysed and *APOGEE* spectra deserve further spectroscopic observations and theoretical considerations. They highlight that stellar compositions remain a challenging pursuit.

8 CONCLUDING REMARKS

Semi-regular red giant variables such as those in Table 1 likely owe their variability to non-radial pulsations of primarily long-period and low amplitude. Variability is thus a natural phenomenon expected of all giants with a photometric amplitude increasing with decreasing effective temperature, that is from G to K to M type (e.g., Jorissen et al. (1997); Henry et al. (2000)). Detailed observational photometric and/or radial velocity variability studies of these red giants provide an interior probe allowing a distinction to be made between a star evolving up the red giant branch and one post He-core flash and now on the asymptotic giant branch.

Our goal with this abundance analysis of a selection of K giant SRd and SRd: variables was to search for abundance differences among elements of Na and heavier between our sample of cataloged semi-variables and similar K giants thought to be photometrically constant. Henry et al. (2000) report that many K giants are photometrically constant at about the 0.002 mag level. To the precision of the spectroscopic abundance analyses – optical and infrared – the elemental abundances of semi-variable giants drawn from the Galactic halo, thick and thin disks show no systematic differences with the (apparently) photometrically constant red giants from the same Galactic population.

It remains to be seen if these seemingly photometrically contrasting groups of K giants show abundance differences for elements lighter than Na, as, for example, Li, C, N, O and F and their isotopes. Some differences are anticipated, if only, because the sample of giants may include stars from both red giant and asymptotic giant branch and the associated evolutionary structural changes (e.g., the He-core flash marking the birth of the low-mass asymptotic giant branch giant) may result in light element and isotopic abundance changes within a giant’s atmosphere. Thorough spectroscopic investigation of M-type giants near the tip of the red giant branch and along the asymptotic giant branch calls for high-resolution infrared spectra as provided by *APOGEE* and *IGRINS* (Park et al. 2014; Yuk et al. 2010) but the intriguing element Li, which eludes the infrared observer, demands an optical spectrum!

⁶ <https://www.sdss4.org/dr17/irspec/abundances/>

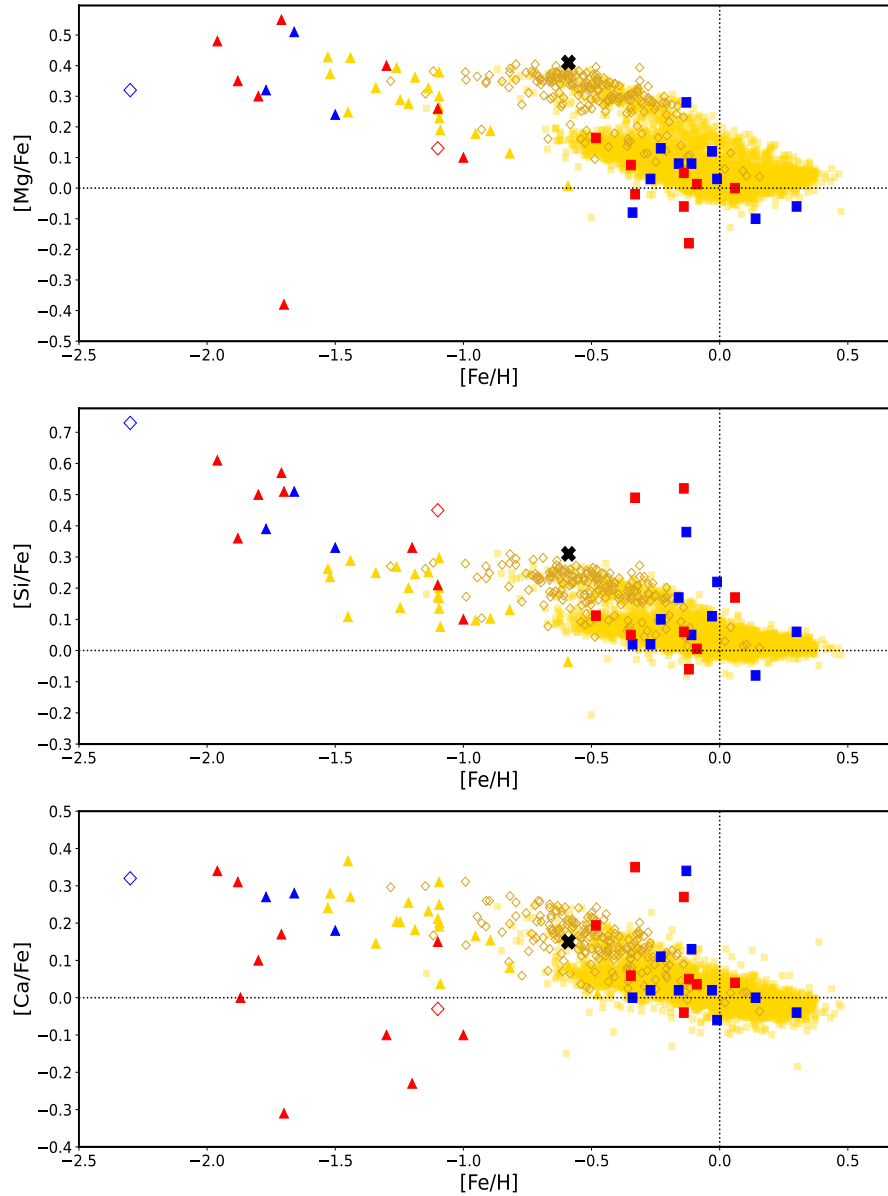


Figure 1. Plots of the abundance ratio $[M/Fe]$ of Mg, Si and Ca against $[Fe/H]$ are shown for the three Galactic populations: thin disk by filled squares, thick disk by open diamonds and halo by filled triangles. Our current SRd variables are represented in blue, previously published SRd variables in red and *APOGEE* giants are coloured yellow. Arcturus is represented by the black X.

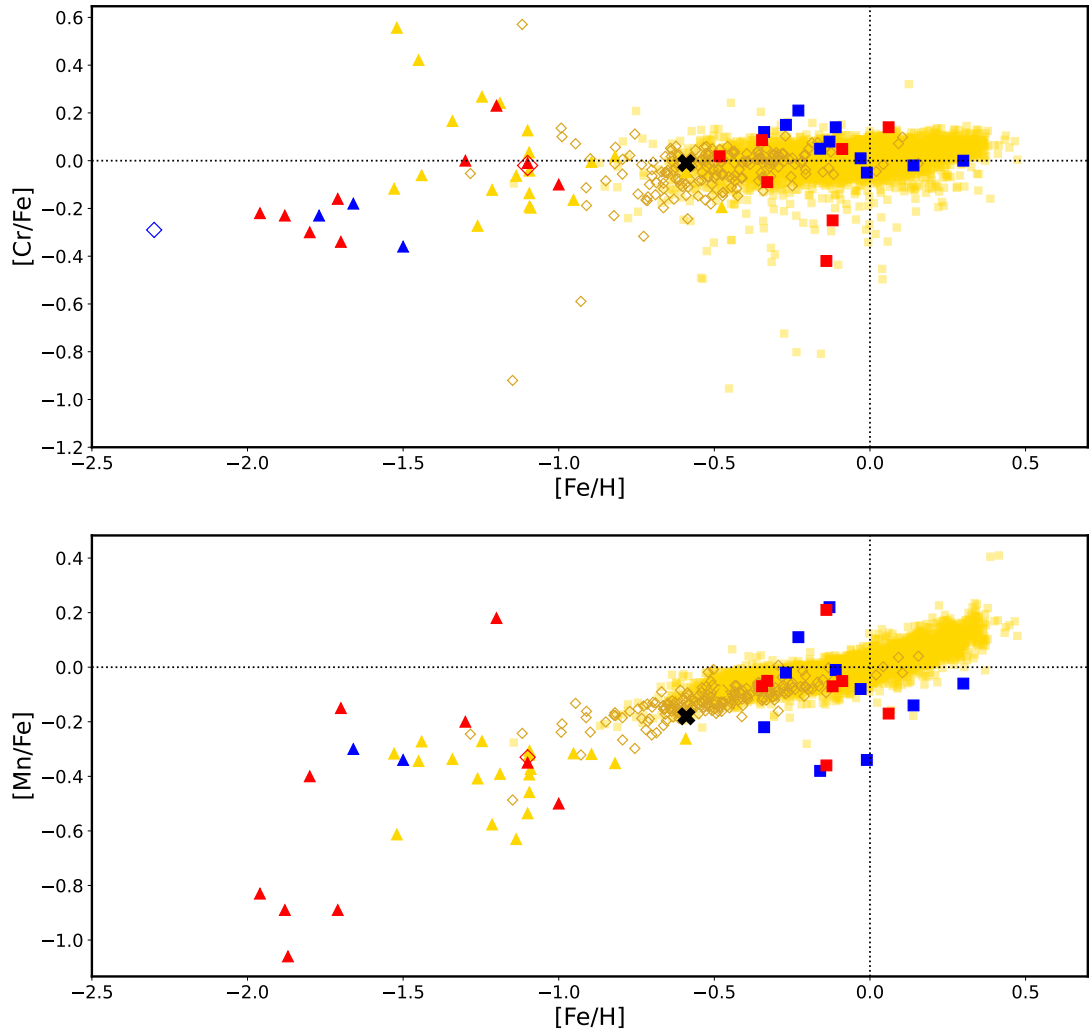


Figure 2. Abundance ratio $[M/Fe]$ of Cr and Mn against $[Fe/H]$. Symbols and colour codes are the same as in the previous figure.

DATA AVAILABILITY

The Survey data used in this article can be accessed at the following links.

SDSS DR17 for APOGEE catalog :

https://data.sdss.org/sas/dr17/apogee/spectro/aspcap/dr17/synspec_lte/allStar-dr17-synspec_lte.fits

LAMOST DR8 Medium Resolution Catalog :

<http://www.lamost.org/dr8/>

GAIA DR3 catalog :

<https://gea.esac.esa.int/archive/>

ACKNOWLEDGEMENTS

We thank our friend N. Kameswara Rao for his suggestion that SRd variables were worthy of pursuit with the *Robert G. Tull* spectrograph. We note too with much appreciation the insights into the voluminous records of the *APOGEE* project volunteered by Carlos Allende Prieto and Verne V Smith. We thank the referee for a thoughtful review.

This work has made use of data from the European Space Agency (ESA) mission *Gaia* (<https://www.cosmos.esa.int/gaia>), processed by the *Gaia* Data Processing and Analysis Consortium (DPAC, <https://www.cosmos.esa.int/web/gaia/dpac/consortium>). Funding for the DPAC has been provided by national institutions, in particular the institutions participating in the *Gaia* Multilateral Agreement.

Guoshoujing Telescope (the Large Sky Area Multi-Object Fiber Spectroscopic Telescope LAMOST) is a National Major Scientific Project built by the Chinese Academy of Sciences. Funding for the project has been provided by the National Development and Reform Commission. LAMOST is operated and managed by the National Astronomical Observatories, Chinese Academy of Sciences.

Funding for the Sloan Digital Sky Survey IV has been provided by the Alfred P. Sloan Foundation, the U.S. Department of Energy Office of Science, and the Participating Institutions.

SDSS-IV acknowledges support and resources from the Center for High Performance Computing at the University of Utah. The SDSS website is www.sdss4.org.

SDSS-IV is managed by the Astrophysical Research Consortium for the Participating Institutions of the SDSS Collaboration including the Brazilian Participation Group, the Carnegie Institution for Science, Carnegie Mellon University, Center for Astrophysics — Harvard & Smithsonian, the Chilean Participation Group, the French Participation Group, Instituto de Astrofísica de Canarias, The Johns Hopkins University, Kavli Institute for the Physics and Mathematics of the Universe (IPMU) / University of Tokyo, the Korean Participation Group, Lawrence Berkeley National Laboratory, Leibniz Institut für Astrophysik Potsdam (AIP), Max-Planck-Institut für Astronomie (MPIA Heidelberg), Max-Planck-Institut für Astrophysik (MPA Garching), Max-Planck-Institut für Extraterrestrische Physik (MPE), National Astronomical Observatories of China, New Mexico State University, New York University, University of Notre Dame, Observatório Nacional / MCTI, The Ohio State University, Pennsylvania State University, Shanghai Astronomical Observatory, United Kingdom Participation

Group, Universidad Nacional Autónoma de México, University of Arizona, University of Colorado Boulder, University of Oxford, University of Portsmouth, University of Utah, University of Virginia, University of Washington, University of Wisconsin, Vanderbilt University, and Yale University.

REFERENCES

- Abdurro'uf., Accetta K., et al., 2022, *ApJS*, 259, 35
 Andrievsky S. M., Korotin S. A., Martin P., 2007, *A&A*, 464, 709
 Andrievsky S. M., Makarenko E. N., Fenina Z. N., 1985, *Problemy Kosmicheskoi Fiziki*, 20, 60
 Arcones A., & Thielemann F.-K., 2023, *A&ARv*, 31, 1
 Asplund M., Grevesse N., Sauval A. J., Scott P., 2009, *ARA&A*, 47, 481
 Babusiaux C., Fabricius C., et al., 2023, *A&A*, 674, A32
 Barklem P. S., Christlieb N., et al., 2005, *A&A*, 439, 129
 Beaton R. L., Oelkers R. J., et al., 2021, *AJ*, 162, 302
 Bensby T., Feltzing S., Lundström I., 2003, *A&A*, 410, 527
 Bowen I. S., Vaughan A. H., 1973, *Appl. Opt.*, 12, 1430
 Britavskiy N. E., Andrievsky S. M., Korotin S. A., Martin P., 2010, *A&A*, 519, A74
 Britavskiy N. E., Andrievsky S. M., Tsymbal V. V., Korotin S. A., Martin P., Andrievska A. S., 2012, *A&A*, 542, A104
 Bubar E. J., King J. R., 2010, *AJ*, 140, 293
 Gaia Collaboration et al., 2016, *A&A*, 595, A1
 Gaia Collaboration et al., 2023, *A&A*, 674, A1
 García Pérez A. E., Allende Prieto C., et al., 2016, *AJ*, 151, 144
 Giridhar S., Lambert D. L., Gonzalez G., 1998, *PASP*, 110, 671
 Giridhar S., Lambert D. L., Gonzalez G., 1999, *PASP*, 111, 1269
 Giridhar S., Lambert D. L., Gonzalez G., 2000, *PASP*, 112, 1559
 Giridhar S., Rao N. K., Lambert D. L., 1994, *ApJ*, 437, 476
 Gunn J. E., Siegmund W. A., et al., 2006, *AJ*, 131, 2332
 Hekker S., Meléndez J., 2007, *A&A*, 475, 1003
 Henry G. W., Fekel F. C., Henry S. M., Hall D. S., 2000, *ApJS*, 130, 201
 Hinkle K., Wallace L., Valenti J., Harmer D., 2000, *Visible and Near Infrared Atlas of the Arcturus Spectrum 3727-9300 Å* (San Francisco: ASP)
 Holtzman J. A., Harrison T. E., Coughlin J. L., 2010, *Advances in Astronomy*, 2010, 193086
 Imig J., Price C., et al., 2023, *ApJ*, 954, 124
 Johnson D. R. H., Soderblom D. R., 1987, *AJ*, 93, 864
 Jönsson H., Allende Prieto C., et al., 2018, *AJ*, 156, 126
 Jönsson H., Holtzman J. A., et al., 2020, *AJ*, 160, 120
 Jorissen A., Mowlavi N., Sterken C., Manfroid J., 1997, *A&A*, 324, 578
 Majewski S. R., Schiavon R. P., et al., 2017, *AJ*, 154, 94
 McWilliam A., 1998, *AJ*, 115, 1640
 Morel T., Miglio A., et al., 2014, *A&A*, 564, A119
 Park C., Jaffe D. T., et al., eds, *Ground-based and Airborne Instrumentation for Astronomy V* Vol. 9147 of Society of Photo-Optical Instrumentation Engineers (SPIE) Conference Series, Design and early performance of IGRINS (Immersion Grating Infrared Spectrometer). p. 91471D

- Perryman M. A. C., et al., 1997, *A&A*, 323, L49
- Pompéia L., Masseron T., et al., 2011, *MNRAS*, 415, 1138
- Ramírez I., Allende Prieto C., 2011, *ApJ*, 743, 135
- Ramya P., Reddy B. E., Lambert D. L., 2012, *MNRAS*, 425, 3188
- Ramya P., Reddy B. E., Lambert D. L., 2019, *MNRAS*, 484, 125
- Ramya P., Reddy B. E., Lambert D. L., Musthafa M. M., 2016, *MNRAS*, 460, 1356
- Reddy B. E., Lambert D. L., Allende Prieto C., 2006, *MNRAS*, 367, 1329
- Reddy B. E., Tomkin J., Lambert D. L., Allende Prieto C., 2003, *MNRAS*, 340, 304
- Samus' N. N., Kazarovets E. V., Durlevich O. V., Kireeva N. N., Pastukhova E. N., 2017, *Astronomy Reports*, 61, 80
- Santana F. A., Beaton R. L., et al., 2021, *AJ*, 162, 303
- Shetrone M., Bizyaev D., et al., 2015, *ApJS*, 221, 24
- Smith V. V., Bizyaev D., et al., 2021, *AJ*, 161, 254
- Snedden C. A., 1973, PhD thesis, University of Texas, Austin
- Tull R. G., MacQueen P. J., Snedden C., Lambert D. L., 1995, *PASP*, 107, 251
- Weinberg D. H., Holtzman J. A., et al., 2022, *ApJS*, 260, 32
- Wilson J. C., Hearty F. R., et al., 2019, *PASP*, 131, 055001
- Worley C. C., Cottrell P. L., Freeman K. C., Wylie-de Boer E. C., 2009, *MNRAS*, 400, 1039
- Yuk I.-S., Jaffe D. T., et al., eds, Ground-based and Airborne Instrumentation for Astronomy III Vol. 7735 of Society of Photo-Optical Instrumentation Engineers (SPIE) Conference Series, Preliminary design of IGRINS (Immersion GRating INfrared Spectrograph). p. 77351M
- Zasowski G., Cohen R. E., et al., 2017, *AJ*, 154, 198